Hindawi
Advances in Civil Engineering
Volume 2020, Article ID 8881416, 13 pages
https://doi.org/10.1155/2020/8881416

Research Article

Mechanical Behavior and Energy Evolution of Sandstone considering Slenderness Ratio Effect

Bibo Dai,[1,2] Xingdong Zhao,[1] Shuwen Zhang,[3] Qian Kang,[3] and Zhonghua Zhu[3]

[1]*Geomechanics Research Center, Northeastern University, Shenyang, Liaoning 110819, China*
[2]*State Key Laboratory of Safety and Health for Metal Mines, Maanshan, Anhui 243000, China*
[3]*School of Resources & Environment and Safety Engineering, University of South China, Hengyang, Hunan 421001, China*

Correspondence should be addressed to Shuwen Zhang; zhangshw1989@sina.com

Received 23 August 2020; Revised 26 November 2020; Accepted 30 November 2020; Published 14 December 2020

Academic Editor: Yixian Wang

To study the influence of slenderness ratio effect on the mechanical behavior, acoustic emission properties, and energy evolution of sandstone, the uniaxial compression tests coupled with acoustic emission technology are carried out at different slenderness ratios D (0.5, 1.0, 1.5, 2.0, 3.0). The results show that a logarithmic function relationship is observed between the peak strength, the peak strain, and the elastic modulus with slenderness ratio. The failure patterns of the tested sandstone varied significantly with the increasing slenderness ratio. When the slenderness ratio, D, is lower than 1.5, complex failures and multiple shear planes are formed, while simple failures and single shear planes are generated at D larger than 1.5. Besides, the AE ringing counts are more obvious with a higher slenderness ratio, D, at the initial compression stage due to the greater body volume and more defects in the sandstone. The energy evolution curves and energy ratio distribution curves can be divided into four stages, corresponding to the stress-strain curves.

1. Introduction

Most underground engineering, such as underground deposit mining, geothermal exploitation, nuclear waste storage, oil boreholes, and tunnel excavation, is highly dependent on proper knowledge of the strength and deformability parameters of rocks [1–4]. The design and stability evolution of such structures requires a deep insight into the strength and deformation behaviors of these rock materials. However, the reliable characterization of such rock parameters with an adequate level of confidence has still remained a challenging issue for rock engineers and researchers. The challenge mainly originates from the highly heterogeneous and discontinuum nature of a specific rock, due to the existence of distributed discontinuities of various sizes from nanometer to centimeter scale pores and cracks and the mineral grains to meso- and macroscale features existing in rocks; the differences in the amount, size, shape, connectivity, and distribution of those characteristics in rocks are closely related to the macrostrength [5]. As a result, the mechanical properties of a rock mass are controlled by both the rock types and the preexisting discontinuities structure surface. In addition, the size of the engineering structure usually far exceeds the size of the laboratory test specimen size. Thus, in view of the presence of discontinuities of various nature and sizes, together with the nonlinear behavior of intact rock mass, the mechanical properties of a specific rock is highly specimen geometry dependent [6].

The specimen geometry is one of the significant influence factors in brittle, quasibrittle, and soft rock with the shape of specimens varying, such as cylindrical, cubic column, triangular column, and the slenderness ratio ranging from 1.0 to 3.0 [7–11]. Changes in strength due to the size effect are significant in the range of about 20 mm to 200 mm in diameter, and specimens smaller than about 50 mm exhibit a large deviation [6]. Many studies have explored the specimen geometry with regard to the uniaxial compression test in different rock types [12, 13] due to the fact that the uniaxial compression strength is often an indispensable

parameter for the stability evaluation of underground engineering. For example, in the field of mining engineering, the relationship between strength and size, mainly for coal, ore, and other surrounding rocks, is actively studied through laboratory and in situ tests in response to the need for its practical application in fields such as the underground excavation design of room and pillar [14]. Zhang et al. [4] used a case study of an underground excavation to identify structural domains, which are highly affected by specimen geometry, and verified that the specimen geometry is an important consideration in structure. One of the first works to systematically study the relative strengths and stability of coal pillars considering specimen geometry was the research carried out by Steart in 1954 [15]. The research shows that the strengths per unit-area of coal pillars of constant width vary in inverse ratio to height, while the strengths per unit-area of coal pillars of constant height vary as the square root of their widths, and the strengths per unit-area of coal pillars of cube form vary in inverse ratio to the square root of their dimensions. Moreover, the elastic modulus (E) at 50% and 70% of failure stresses shows a decreasing tendency as the specimen size increases. Previous studies have shown that the uniaxial compression strength of hard rock decreases as specimen size increases [16]. Unlike the hard rocks, saliferous rocks are notable for a directly contrary manifestation of the scale effect; that is, when the linear sizes of the sample increase, the ultimate compression strength also increases [17], and it is stabilized when the sample's size is greater than 10 cm [18]. In addition, other researchers also find that the specimen geometry on soft rock is generally not significant, and the correlation of uniaxial compression strength values in different diameters with estimations of specimen size effect models was weak [19]. To sum up, the specimen geometry is manifested differently depending on the rock type [20], and it needs further study considering different kinds of rocks.

Although the specimen geometry influences the magnitude of strength, the specimen geometry can be estimated from the ratio of strength in the case of specimens with the same samples. In general, two types of specimen geometry effect are considered to be relevant, namely, size effect and shape effect. Size effect basically refers to the influence of the absolute size (i.e., side length and diameter) of the rock specimen, which has a constant slenderness rate while the shape effect mainly contains the influence of the slenderness ratio of the rock specimen on strength behavior [21]. As a rule, the length-to-diameter ratio (D = length/diameter) for a cylindrical specimen or the height-to-width ratio for a plane strain specimen is regarded as slenderness ratio [22], and the analytical methods for shape effect can be divided into three categories: statistical theories based on Weibull theories, empirical and semiempirical models, and theories based on fracture mechanics [23]. Much of the research has been based on specimens of nonstandard dimensions and shapes and over a limited size range as summarized by Liang et al. [24]. Masooumi et al. [12] proposed a multiaxial failure criterion for intact rock incorporating shape effect and found some parameters in the criterion are shape-dependent. Zhang et al. [3] validate the capability of the combined finite-discrete element method code to accurately represent in situ pillar behavior and to evaluate the relationship between microparameters calibrated at the laboratory-scale and the field-scale. In a word, the results from previous laboratory studies showed that the rock strength generally decreased as the slenderness ratio increased, and the strength would become a constant value when the slenderness ratio increased to a threshold [25–28]. In addition, a series of models between sample size of rock and strength have been proposed through statistical analysis and theoretical analysis [6]. In order to obtain the reliable laboratory test results of the rock strength, the shape of rock specimens was required by different authorities [29, 30] with a slenderness ratio of 2.0 to 3.0. However, the damage evolution of rock at the mechanical tests with different slenderness ratios is still unclear. Thus, to better understand the mechanical behaviors of rocks and apply to the design of larger rock structures, laboratory experimental investigations considering shape effect are still necessarily needed to further study, and it is worth estimating the strength characteristics of actual intact rock with the shape effect models.

In this study, a series of uniaxial compression tests coupled with acoustic emission technology have been designed and performed at different slenderness ratios D (D = 0.5, 1.0, 1.5, 2.0, 3.0 with the constant diameter of about 50 mm) to explore the mechanical behavior and energy evolution of sandstone considering slenderness ratio effect. The changes and the relationship between peak strength, the peak stain, the elastic modulus, and the slenderness ratio were documented and analyzed. The failure patterns and the energy characteristics were investigated in detail. This study provided new insights into the mechanical behavior and energy evolution of sandstone with different slenderness ratios, and it has the potential to obtain reliable rock parameters for the underground engineering design and construction.

2. Test Materials and Equipment

Sandstone sampled from Zigong, Sichuan province of China, was used. The mercury intrusion porosimetry test showed that porosity is 5.8%. The P- and S-wave velocities of the sandstone are 2950 m/s and 2072 m/s, respectively, which indicated the sandstone significant anisotropy inducing the different mechanical characteristics. The X-ray diffraction analysis implied that the mineral components mainly consist of quartz (58%), feldspar (15), and clay (11%), and the content of brittle minerals is more than half. The microscopic structure of the tested sandstone based on scanning electron microscopic (SEM) is shown in Figure 1, showing that the grains are randomly distributed; micropores and microcracks are observed among the grains, which may lead to less strength under the uniaxial compression tests. In addition, the trace of slip is discovered in Figure 1, suggesting that shear failure occurred. All of the tested specimens were drilled perpendicular to the same side of the same sandstone block with a diameter of 52 mm drilling tube and drilled into the cylinder shapes with a constant diameter of about 50 mm. Then, cut the drilled specimens into the

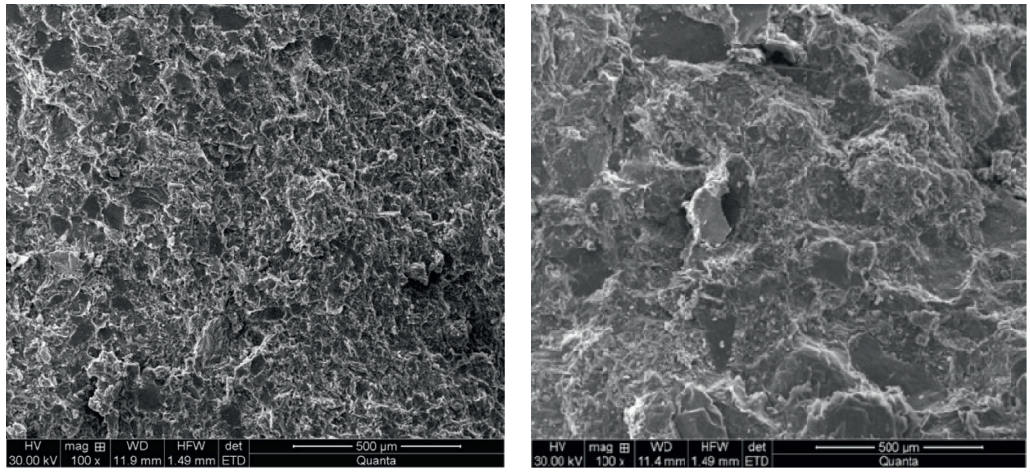

(a) (b)

Figure 1: SEM images of sandstone with a magnification of 100 times.

different height-diameter ratios D (0.5, 1.0, 1.5, 2.0, 3.0) and group and label them into five sets. To ensure the specimen is not subjected to biased axial pressure, the two ends of the specimen were parallel to each other for testing. The unevenness of both ends of all the specimens and the height of the same sets of specimens are less than 0.02 mm and 0.2 mm, respectively.

The uniaxial compression test of the sandstone specimens was conducted on the electrohydraulic servo rock mechanics test system RMT-150b independently developed by Wuhan Geotechnical Institute, Chinese Academy of Sciences. This testing system is mainly composed of the axial pressure loading system, confining pressure system, lateral pressure system, controller, and an automatic data acquisition system. The uniaxial compression, triaxial compression, direct tension, and direct shearing can be conducted using this system with the maximum axial pressure, lateral pressure, and shear loading being 1000 kN, 50 MPa, and 500 kN, respectively. All the uniaxial compression tests were carried out with the RMT-150b system using axial displacement control with the loading rate of 0.01 mm/s and coupled with the acoustic emission system.

To identify the damage evolution of the specimen with different slenderness ratios, the AE signals were collected with DS5-8B acoustic emission signal analyzer with 8 channels produced by Beijing Soft Island during the uniaxial compression strength testing. In the strength test, the AE detection threshold value was set at 40 dB and the frequency was set at 140 kHz. To ensure successful signal detection and obtaining, two sensors were installed in the lateral position in the middle of the cylindrical specimen with a rubber band fixing, and the AE signals were collected as the sample was stressed.

3. Results and Discussion

3.1. Stress-Strain Behavior. For each set of uniaxial compression tests, three specimens were performed. The stress-strain curves obtained from those sandstone specimens with different slenderness ratios are shown in Figure 2. It is important to point out that the stress-strain curves of specimens in the same set exhibit a similar trend during the whole loading process, which indicates that the dispersion is relativity low and the data is reliable. As shown in Figure 2, the stress-strain curve of all specimens can be divided into four stages: the initial compression stage, the elastic stage, the yield stage, and the postpeak residual stage.

Take the specimen with the slenderness ratio, $D = 0.5$, as an example (Figure 2). In the initial compression stage, the stress-strain curve presents initially concave up, which is possibly due to the closure of the pore-fracture system such as pores, preexisting microcracks, and defects in the specimens. As the loading increases to the elastic stage, remarkable elastic deformation is formed and the slope of this stage is approximating constant; that is, the stress is proportional to the stain, and the strain can get full recovery after unloading. Passing this elastic stage, the stress-strain curves enter the yield stage. At this stage, the curves become deviate from linear response gradually, which indicates the increasing rate of the strain is greater than that of stress and microcracks generate more and more. This stage is a sign that the destruction of rock has begun, and the nonlinear stress-strain behavior becomes convex up until the peak stress with loading, which is contrary to that of the initial compression state. After reaching the peak stress, the curves drop rapidly to the residual stress level, resulting in significant strain softening, which is the postpeak residual stage. At this stage, microcracks are interconnected and failure becomes nonstable.

Comparing the experiments' date of five sets, the greater the slenderness ratio, the smaller the peak strength (UCS), the peak strain (the peak strain, ε, was defined as the strain value at the peak stress), and the residual strength, and the lager the elastic modulus (E). On the other hand, the steep postpeak slopes of the stress-strain curves suggest that all sandstone specimens exhibit brittle characteristics, which correspond to the brittle minerals it contains. In addition, it illustrates that the residual strength of greater slenderness

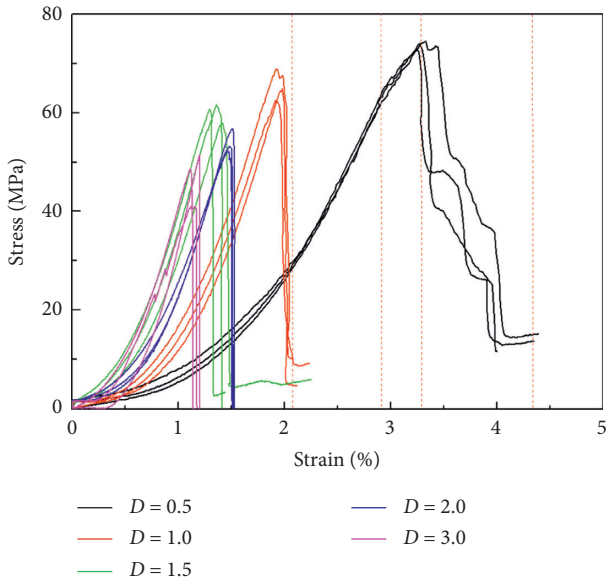

Figure 2: The stress-strain curves of sandstone considering slenderness ratio (D).

ratio is significantly lower than that of smaller slenderness ratio implying that the failure of such specimens can be potentially invalid. On the other hand, specimens with a smaller slenderness ratio can maintain their strength and even exhibit strain hardening behavior after initial yielding. In terms of strain, Figure 2 shows that the specimens with a greater slenderness ratio may lose their load capacity at a lower axial strain. It is important to point out the phenomenon of brittleness is more pronounced with the increase of the slenderness ratio, which indicates that the brittleness characterizes are also related to the shape of the specimen. Based on the observations and analyses in this section, the appropriate shape of the pillar and the timely support should be considered in the actual pillar design and application of mining.

3.2. Effect of Slenderness Ratio on the Mechanical Properties of Sandstone. From all the tests, Table 1 lists the peak strength, the peak strain, and the elastic modulus for the tests considering different slenderness ratios. For each set of slenderness ratio uniaxial compression tests, the mean value of peak strength, the peak strain, and the elastic modulus were calculated from each set of three tests.

For each slenderness ratio set specimens, the average values of UCS are 74.18, 65.47, 60.14, 54.13, and 47.04 MPa at slenderness ratio of 0.5, 1.0, 1.5, 2.0, and 3.0, respectively. The measured data show that specimens with $D = 0.5$ are approximately 94% higher and exhibit a lower postpeak strength reduction compared to that with $D = 3.0$. The strength results show that the effect of slenderness ratio on the strength should not be ignored, and it also supports the importance of accurate measure the strength of specimen and monitors the pillar with the larger slenderness ratio in real engineering. Besides, these strength data and Figure 3 show that a higher slenderness ratio leads to lower peak strength, which indicates that the slenderness ratio has a weak effect on sandstone. A similar phenomenon on peak strength was seen by other researchers [15, 20, 21, 31]; they reported that the mechanical properties of a rock mass are controlled by both the behavior of preexisting discontinuities and the stress-fracture behavior of intact blocks making up the rock bridges between discontinuities. On the other hand, the nature of the shape effect is that real solid bodies always containing internal defects such as vacancies, dislocations, cracks, and inclusions of microvolumes of different strength randomly distributed within the volume. Therefore, the greater the body's volume is, the more the defects are and the less the strength it has [20]. Besides, discontinuity characteristics, such as orientation, trace length, and spacing, significantly vary across different areas of a rock mass, resulting in different physical and mechanical properties [32]. The fact that the scale effect exists in rocks is explained by various internal defects that concentrate stress, which is manifested in decreasing strength indicators and increasing sizes of samples.

In order to reveal the effect of slenderness ratio on the mechanical properties of tested sandstone, it is useful to qualitatively and quantitatively analyze the relationship between the slenderness ratio and the mechanical parameters.

Through the regression analysis, the relationship between peak strength (UCS) and the slenderness ratio, D, is shown in Figure 3; the UCS as a function of D in a UCS-In (D) plot with $R^2 = 0.91$ is shown in

$$\mathrm{UCS} = a + b^* \ln(D), \tag{1}$$

where a and b are tested sandstone constants which were, respectively, equal to 64.73 and −15.09 for the tested sandstone in this study. These values are for UCS and D, respectively, in the units of MPa and MPa.

The fitting results indicate that the empirical model (equation (1)) is in good agreement with the measured values. It is also worth noting that the slope of equation (1) becomes gentle with the increase in slenderness ratio. For a specimen with an infinitely small slenderness ratio, the strength of this specimen has an infinitely great value, while for the infinitely great slenderness ratio specimen, the strength may be a negative value. However, the idea of infinity is hard to be established in theory and reality. Obviously, the strength could not be a negative value no matter what the slenderness ratio is, which suggests that the empirical model has a certain scope of application. In addition, the largest limit slenderness ratio value can be derived by (1) in reality supposing the strength value equal to zero, and the largest limit slenderness ratio $D_m = 148.40$ in tested sandstone; namely, when the slenderness ratio reaches close to D_m, the strength of tested sandstone would get smaller and smaller until it loses its loading capacity.

Like the peak strength, the regression analysis results of the peak strain and the elastic modulus are shown in Figures 4 and 5. As shown in the figures, a logarithmic function is also observed between the peak strain and the slenderness ratio, as well as the elastic modulus and the

Table 1: Uniaxial compression tests parameters and mean results.

Test number	Slenderness ratio	Peak strain (%)	Peak strength (MPa)	Elastic modulus (GPa)
0.5-1	0.5	3.26	73.86	37.85
0.5-2	0.5	3.24	73.14	36.92
0.5-3	0.5	3.33	75.55	35.96
0.5-mean	0.5	3.28	74.18	36.91
1-1	1	1.92	68.92	63.78
1-2	1	1.91	62.59	60.99
1-3	1	1.98	64.89	61.61
1-mean	1	1.94	65.47	62.13
1.5-1	1.5	1.42	57.97	64.01
1.5-2	1.5	1.36	61.69	69.24
1.5-3	1.5	1.29	60.76	72.20
1.5-mean	1.5	1.36	60.14	68.48
2-1	2	1.48	53.32	65.31
2-2	2	1.48	52.23	61.41
2-3	2	1.51	56.84	65.58
2-mean	2	1.49	54.13	64.10
3-1	3	1.11	48.64	64.58
3-2	3	1.20	51.46	77.16
3-3	3	1.12	41.02	71.14
3-mean	3	1.14	47.04	70.96

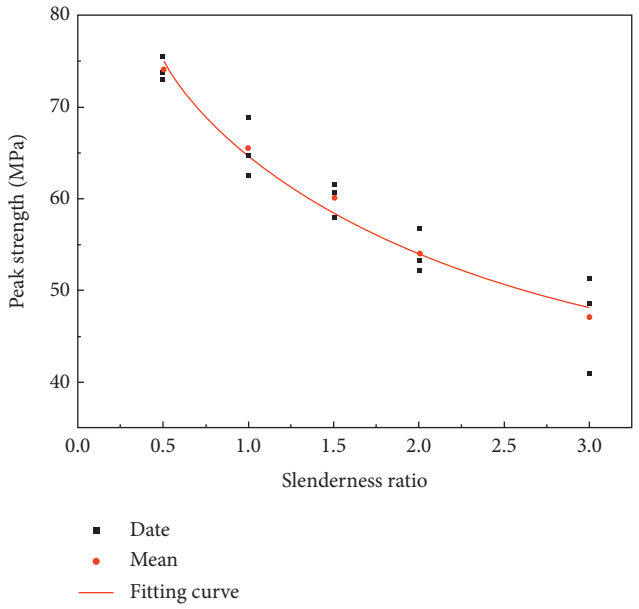

Figure 3: The peak strength versus the slenderness ratio (D).

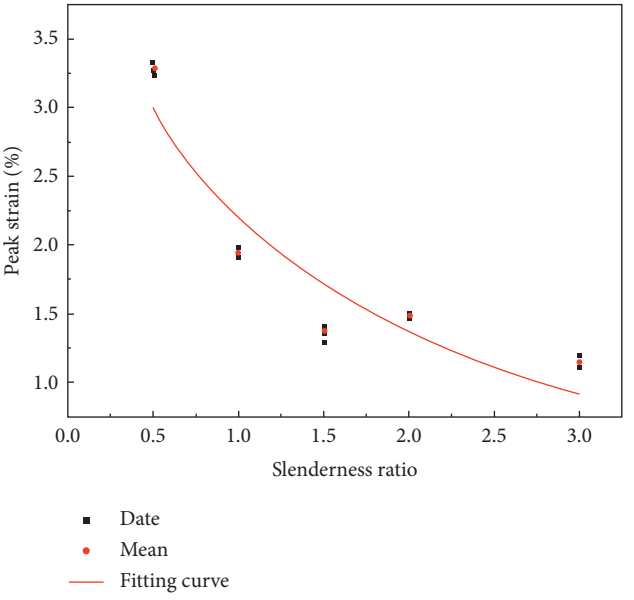

Figure 4: The peak strain versus the slenderness ratio (D).

slenderness ratio, which can be closely represented by the following equations, respectively:

$$\varepsilon = c + d^{*}\ln(D), \tag{2}$$

$$E = e + f^{*}\ln(D), \tag{3}$$

where c, d, e, and f are tested sandstone constants which were, respectively, equal to 2.19, 1.17, 55.15, and −17.85 for the tested sandstone in this study. These values are for ε, E, and D, respectively, in the units of %, %, GPa, and GPa.

Combining the regression analysis results of the relationship between the slenderness ratio and mechanical parameters, a general formula can be drawn as follows:

$$Y = A + B^{*}\ln(D), \tag{4}$$

where Y represents the mechanical parameter, UCS, ε, and E. A and B are tested sandstone constants.

Failure patterns of the tested specimens under uniaxial compression tests at different slenderness ratios are shown in Figure 6 (taking the typical failure patterns as an example). When the slenderness ratio, D, is lower than 1.5, complex failures are formed, and the fracture planes come across the whole specimen and reach the end face showing multiple-plane shear phenomenon, resulting in complex fracture networks. Some fracture planes even come across the end face of the specimens (Figures 6(a)–6(c)) with visible sandstone local fall-blocks at the side of specimens, which

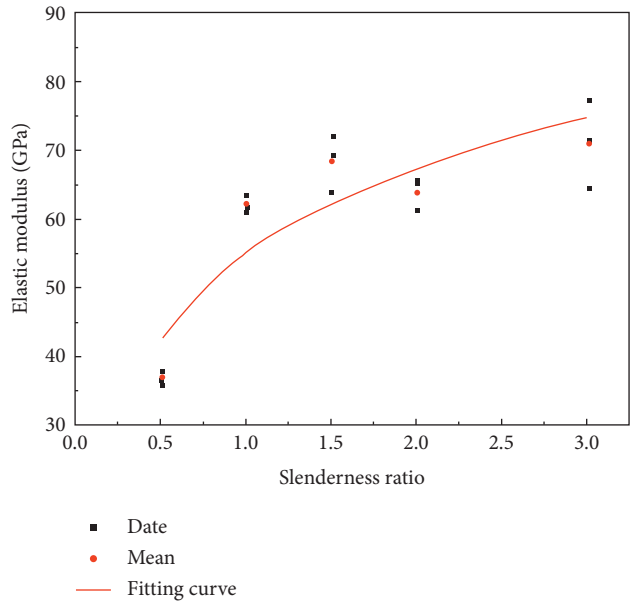

Figure 5: The elastic modulus versus the slenderness ratio (D).

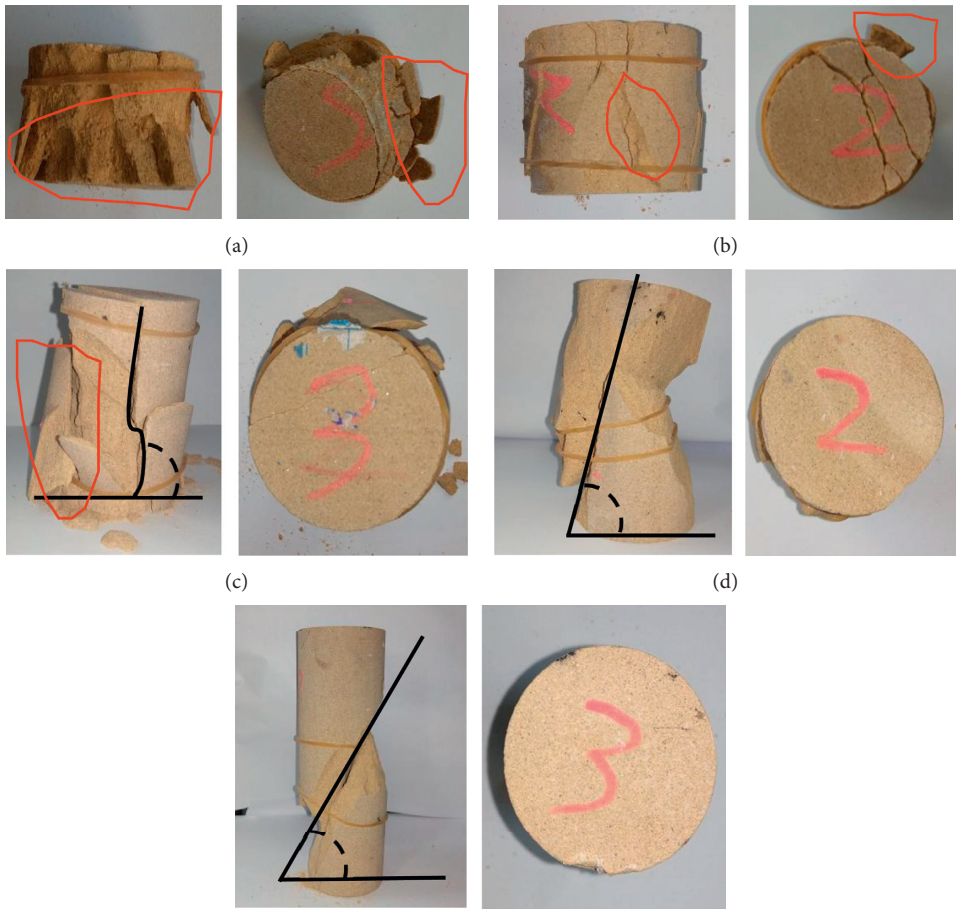

Figure 6: The failure characteristics versus the slenderness ratio (the red regions represent the location of fall-blocks, the angles made up of two black lines represent the angle between those two failed zones and horizontal axis). (a) $D = 0.5$. (b) $D = 1.0$. (c) $D = 1.5$. (d) $D = 2.0$. (e) $D = 2.0$.

indicates those fractures are caused by the tensile stress due to the splitting effect. In addition, the angle between the failure surface and horizontal axis is about 90°, and the number of fracture planes and fracture morphology seems to decrease with the slenderness ratio increasing. With the slenderness ratio increasing, the fracture planes are presenting a tendency of inclining and the fracture morphology becomes simple (Figures 6(d) and 6(e)) showing single-plane shear phenomenon, and two failed zones are generated forming two distinct breakouts on the sides of the specimens. The angle between those two failed zones and horizontal axis becomes lower with the slenderness ratio increasing which indicates the failure slip along the fracture plane.

3.3. Effect of Slenderness Ratio on Acoustic Emission Properties of Sandstone. In the aspect of damage monitoring of the rock mass failure, AE technology was widely applied. Notably, the AE technology could detect the damage inside the rock mass. For a better understanding of the slenderness effect on the sandstone, the characteristics of AE signals were analyzed in this study. In view of the slenderness effect, the relationship between AE ringing count, the cumulative AE ringing count ($\sum$AE), and stress with time is shown in Figure 7 (taking the typical failure patterns as an example).

The relationship between the AE ringing count, the cumulative AE ringing count, and stress with time is shown in Figure 7. The AE sensor was not installed and AE parameters were not detected at the specimen with slenderness ratio $D = 0.5$ due to difficulty in the sensor installing. When the slenderness ratio $D = 1.0$, a small number of AE ringing counts begin to appear at the initial compression stage, and the AE signals with low ringing count level are mainly caused by the compaction between minerals structure and the original defects of the tested specimen (Figure 7(a)). Then, the AE ringing counts are kept relatively stable at a low level with continuous axial loading at the elastic stage. During the yield stage, the stress of the specimen is redistributed, and the microcracks generated in the specimen extend up and down into macrocracks, the AE ringing counts are maintained at a high level. During the stress reaching the peak stress, the AE ringing count suddenly increases and reaches the maximum value, those macrocracks become increasingly wide and long, and the specimen loses its bearing capacity. Then, the AE ringing count slows down to a low level at the postpeak residual stage; there are almost no signals detected. For the cumulative AE ringing count ($\sum$AE), the $\sum$AE raised gradually before the stress reaches the peak strength, which indicates the damage occurs in the whole process. When the stress reaches the peak strength, the leaping growth occurs, which suggests the specimen is destroyed. As for the acoustic emission properties of sandstone at the slenderness ratios $D = 1.5$ and $D = 2.0$, they show a similar trend (Figures 7(b) and 7(c)). The AE ringing counts are more than that of $D = 1.0$ at the initial compression stage; this phenomenon is more significant at the slenderness ratio $D = 3.0$ (Figure 7(d)), which is because the greater the body's volume is, the more defects and the less strength it has [20]. Due to the more defects at the specimens with higher slenderness ratio, the larger destruction displacement is required, that is, more time is needed in the test with higher slenderness ratio under the same loading rate. While there is less AE ringing counts occur at the near of peak stress, which indicates less fracture generation corresponding to the failure pattern in Figure 6. During the whole process, the $\sum$AE increases rapidly at the beginning with the higher slenderness ratio, then creeping up linearly at a roughly constant increasing rate (Figures 7(b)–7(d)).

3.4. Effect of Slenderness Ratio on Energy Accumulation and Dissipation of Sandstone. It is emphasized that the failure and damage of the sandstone are processes, in which energy accumulation, release, and dissipation occur simultaneously. Assuming there is no heat exchange between the physical process and the external environment during the uniaxial compression test. It can be considered that all the external force work is transformed into energy storage, the strain energy released during loading plays a vital role in the destruction of rock and the energy dissipation produce damage and irreversible deformation inside the rock and makes the rock eventually fail; namely, rock failure and damage are processes of energy accumulation and dissipation.

The total strain energy, U, the recovery elastic strain energy, U^e, and the dissipated energy, U^d, of rocks can be expressed as follows in the uniaxial compression test [32]:

$$U = U^e + U^d, \tag{5}$$

where the values are for U, U^e, and U^d all in the units of kJ/m^3.

The total strain energy, U, and the recovery elastic strain energy, U^e, in the rock under uniaxial conditions are expressed as the following equations, respectively, in the uniaxial compression test [33]:

$$U = \int \sigma_1 d\varepsilon_1 = \sum_{i=1}^{n} \frac{1}{2} \left(\varepsilon_{1i+1} - \varepsilon_{1i}\right)\left(\sigma_{1i+1} + \sigma_{1i}\right), \tag{6}$$

$$U^e = \frac{1}{2}\sigma_1 \varepsilon_1^e = \frac{\sigma_1^2}{2\overline{E}}, \tag{7}$$

where σ_1 and ε_1 are the stresses and strain, respectively, at any position on the stress-strain curves, $\overline{E}$ is the average value of unloading elastic modulus, which is often replaced by the initial elastic modulus (E) for the convenience of calculation, i refers to the number of incremental segments, n is the total number of incremental trapezoids, ε_{1i+1} and ε_{1i} are coordinate points of the trapezoid in the axial strain direction, and σ_{1i+1} and σ_{1i} are coordinate points in the axial stress direction. For better knowledge about the equation, the relationship between the total strain energy, the dissipated energy, and the elastic energy of the rock element is shown in Figure 8 [34–36].

Converting equation (5), the dissipated energy, U^d, can be expressed as follows:

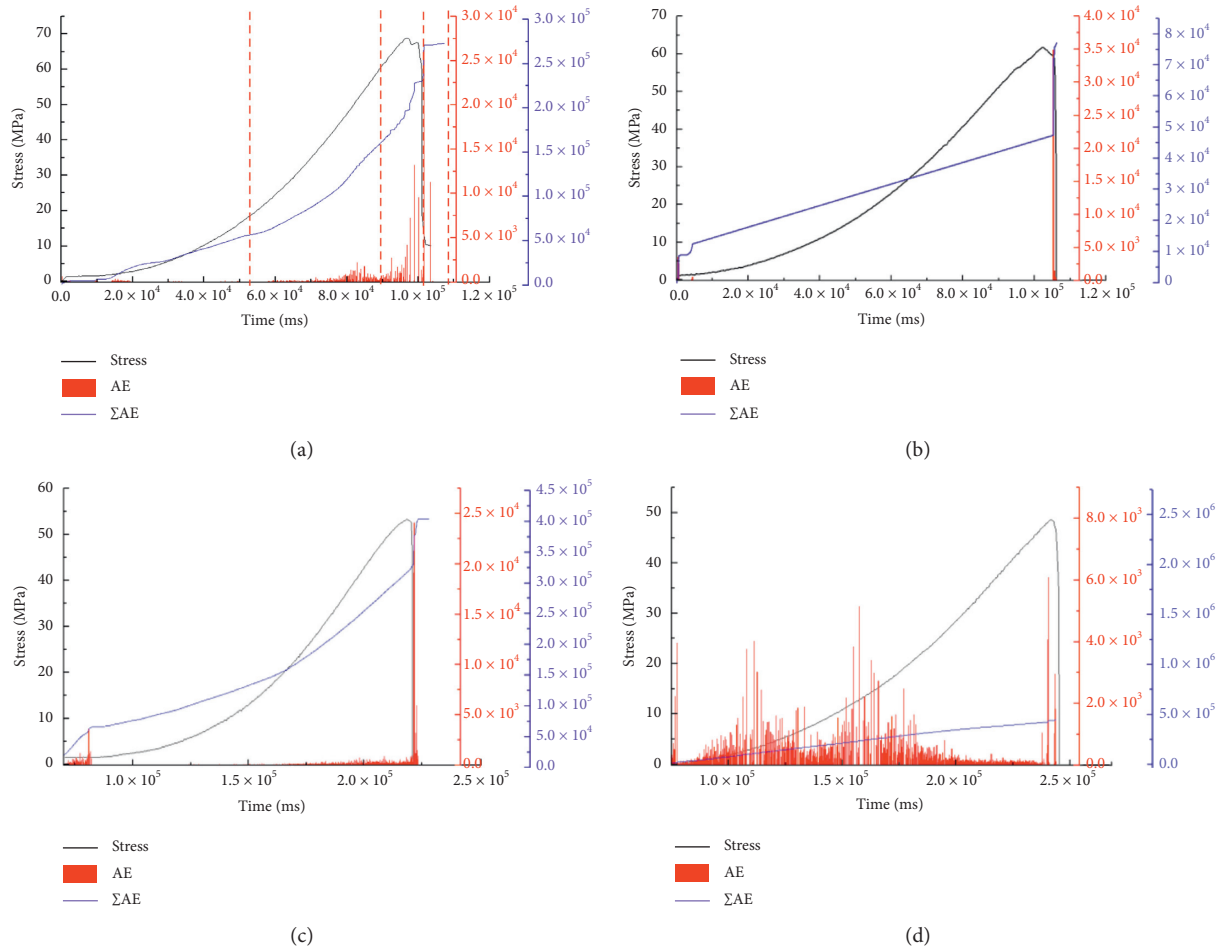

Figure 7: Variation of AE ringing count, the cumulative AE ringing count, and stress with time at different slenderness ratios (D). (a) $D = 1.0$. (b) $D = 1.5$. (c) $D = 2.0$. (d) $D = 3.0$.

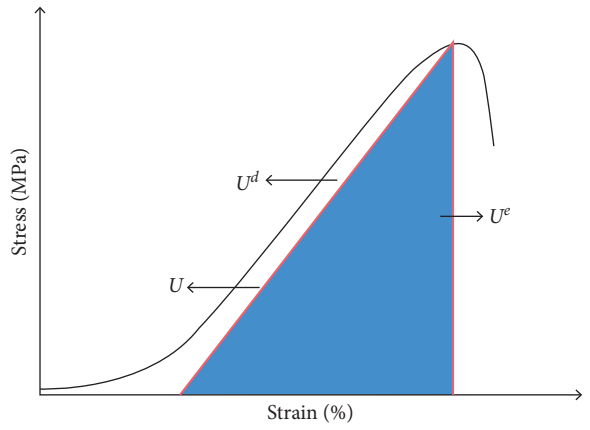

Figure 8: Relationship between the dissipated energy and the elastic energy of the rock element.

$$U^d = U - U^e. \tag{8}$$

For the tested sandstone, based on the equations described above, energy components U, U^e, and U^d can be calculated directly from the stress-strain of uniaxial compression tests (Figure 2). Figure 9 shows U, U^e, and U^d for the different slenderness ratios and it can be seen that energy evolution curves at different slenderness ratios present similar tendency, while the value of each parameter is obviously different, which indicates the slenderness ratio has a significant effect on the energy evolution of the specimen. The U curves increase slowly first, fast afterwards, and very sharply at the peak stress point and then become smooth and steady at last. U^e hardly increases first and fast afterwards, drops sharply at the peak stress point, and then drops down to near zero while U^d increases slowly first and fast afterwards, drops before the yield point, and then increases sharply at last.

For better understanding the energy evolution of the tested sandstone, the energy evolution curves can be divided into four stages corresponding to the stress-strain curves in Figure 2. As shown in Figure 9(a), taking $D = 0.5$ for example, see the following:

Stage 1: It is the initial compression stage of the stress-strain curve (Figures 2 and 9(a)). Energy components U, U^d, and U^e all increase at the low level slowly, of which U^e is smaller than U^d, which is possibly because of the closure of preexisting microcracks and internal defects in the

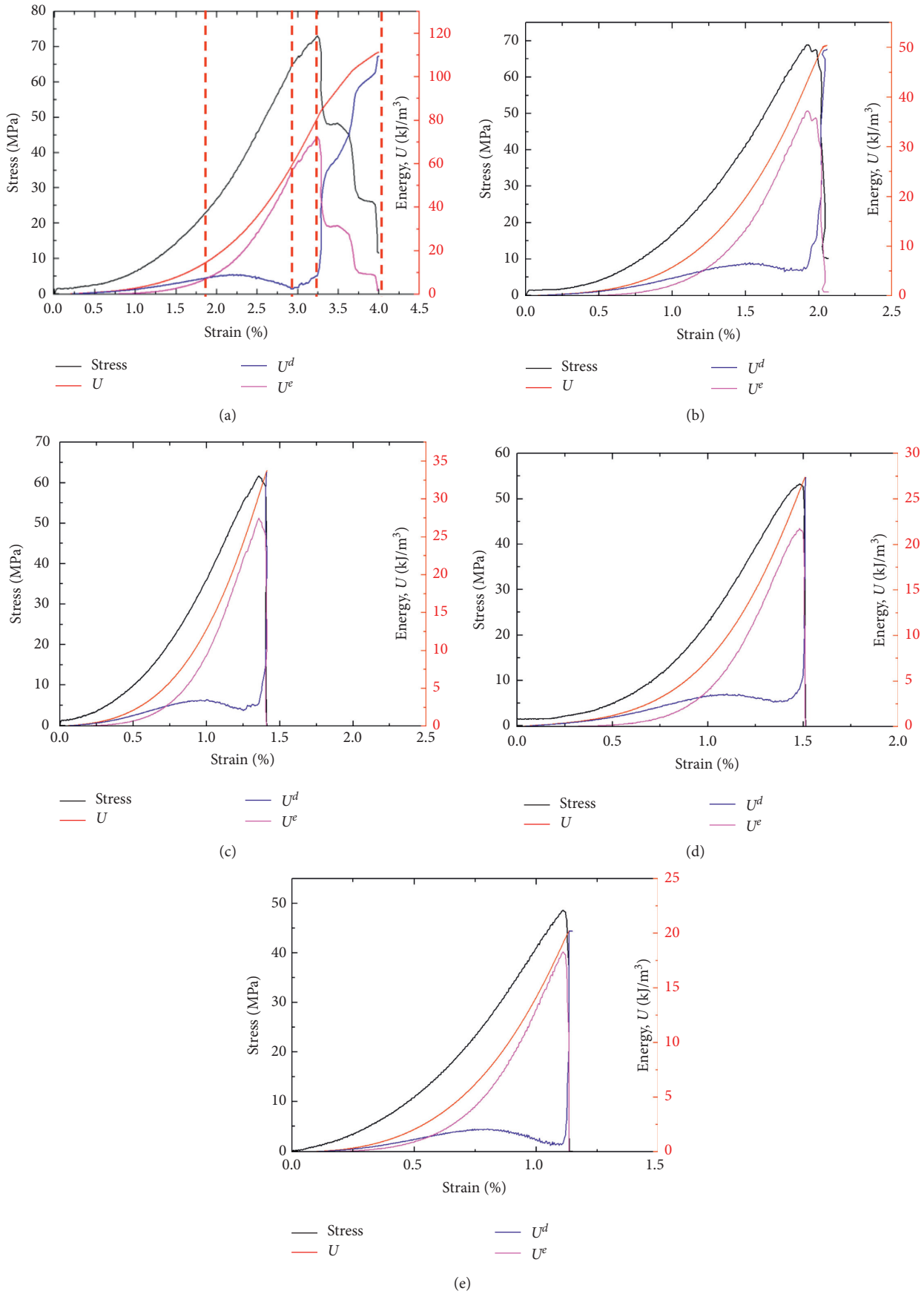

Figure 9: Energy evolution curves under stress at different slenderness ratios. (a) $D = 0.5$. (b) $D = 1.0$. (c) $D = 1.5$. (d) $D = 2.0$. (e) $D = 2.0$.

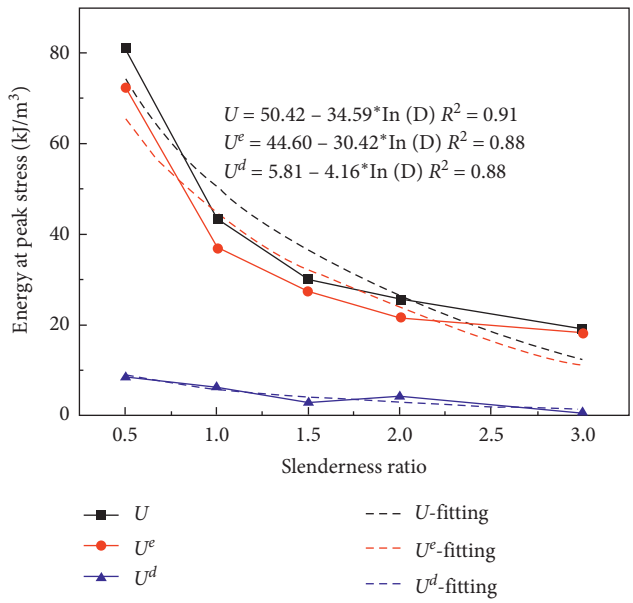

Figure 10: Energy at peak stress versus slenderness ratio.

specimen. At this stage, only an extremely small amount of energy was converted into elastic energy for storage.

Stage 2: It is elastic stage of the stress-strain curve (Figures 2 and 9(a)). Energy components U, U^d, and U^e all present the nonlinear growth pattern due to the stable elastic deformation being generated in the specimen, of which the increasing rate of U and U^e is larger than that of U^d; however, a turning point occurs in U^d at the middle of this stage, and U^d presents concave down. This turning point implies that damage and irreversible deformation inside sandstone mainly occur at the beginning of this stage. The dissipated energy U^d only accounts for a small part of energy and most of the total absorbed energy U is used to convert to the recoverable elastic strain energy U^e. The results reflect that most of the energy is stored in the specimen in the form of recoverable elastic strain energy.

Stage 3: It is the yield stage of the stress-strain curve (Figures 2 and 9(a)). Energy components U, U^d, and U^e all increasing at a high growth rate. As the specimen deformation increases, the energy transforms from linear elasticity into nonlinear elasticity, which is the stable extension of microracks. With those microcracks developing and expanding, U^d suddenly increases until the specimen peak strain is reached and macroscopic damage begins. It is worth noting that the U^e curve is still creeping up until it reaches the limit value at the peak stress, which indicates that the energy is still stored in the specimen due to its overall integrity and loading capacity.

Stage 4: It is the postpeak residual stage of the stress-strain curve (Figures 2 and 9(a)). After passing the peak stress, the growth rate of the U is decreased at the specimen with the lower slenderness ratio, and the majority of energy is consumed for the specimen destruction. Additionally, due to the residual strength of the specimen, there exists a certain amount of elastic energy in this stage, which is different from that with the higher slenderness ratio.

Choosing the typical location of the stress-strain curve, the relationship between slenderness ratio and energy evolution is shown in Figure 10. It can be seen that U, U^d, and U^e are closely related to the slenderness ratio, and the values of U and U^e are much larger than that of U^d at the peak stress. In addition, the logarithmic relationship can be found between U, U^d, and U^e with slenderness ratio, corresponding to the relationship between the mechanical parameters and slenderness ratio, implying that a certain relationship between the mechanical parameters and U, U^d, and U^e may exist.

To facilitate the analysis of the energy mechanism of tested specimens deformation and failure at different slenderness ratios, the ratio of the dissipated energy and the recovery elastic strain energy to the total strain energy at any time during the specimens loading process, which is called the dissipated energy ratio, λ, and the elastic energy ratio, φ, respectively, is

$$\lambda = \frac{U^d}{U}, \tag{9}$$

$$\varphi = \frac{U^e}{U}. \tag{10}$$

The energy distribution curves and stress-strain curves of tested sandstone at different slenderness ratios are illustrated in Figure 11. In the initial compression stage, the energy absorbed by the rock is mainly converted into dissipated energy and reaches the first peak value due to the microcracks and defects compression. As the stress continues, the energy dissipated ratio gradually decreases, and the elastic energy ratio continuously increases. The elastic energy ratio of tested sandstone in the elastic stage maintains stable growth when the proportion of elastic energy reaches the maximum value while the tested sandstone enters the yield point and the yield stage. In this stage, the increasing rate of

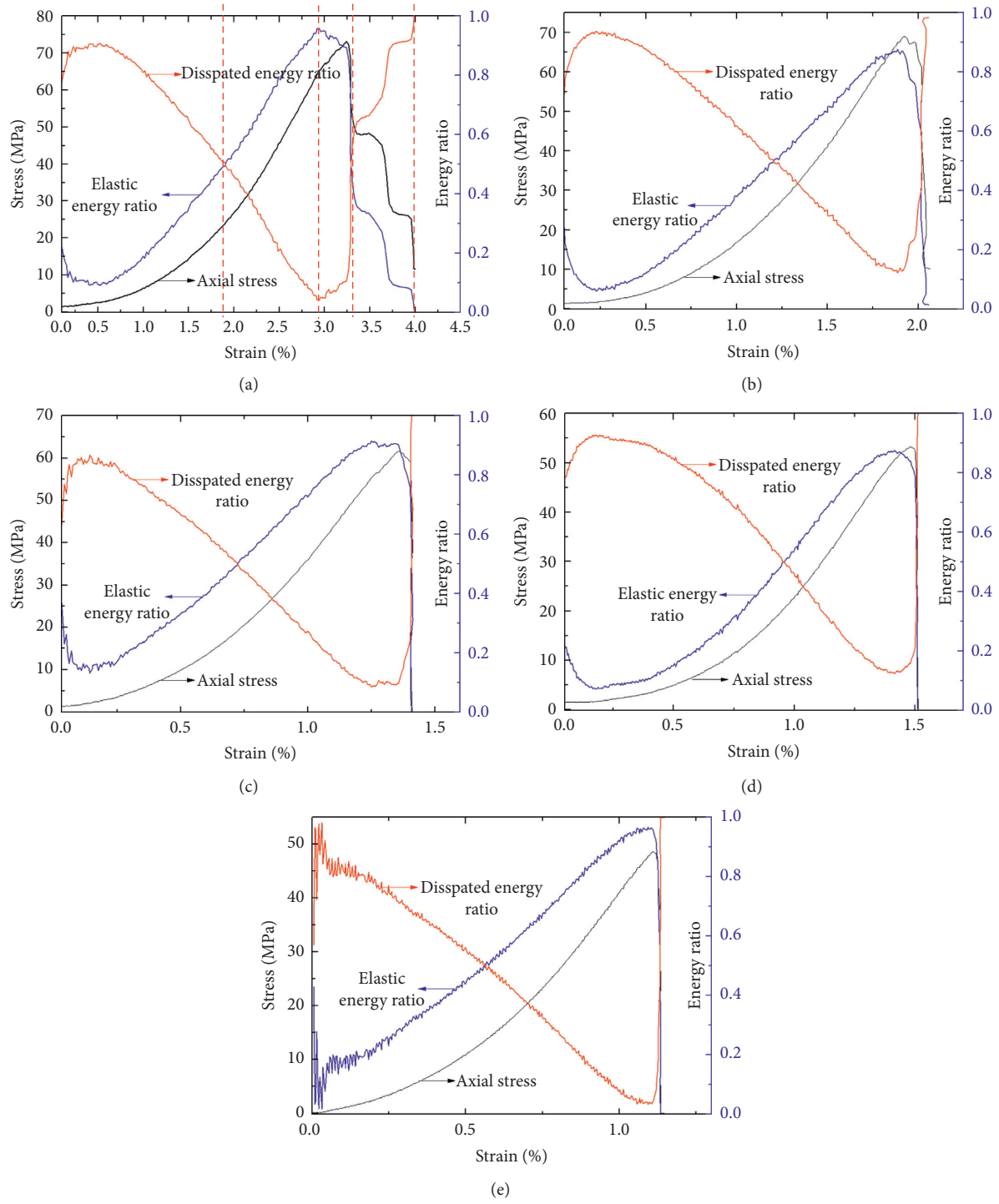

Figure 11: Energy ratio distribution curves and stress-strain curves of sandstone at different slenderness ratios. (a) $D = 0.5$. (b) $D = 1.0$, (c) $D = 1.5$, (d) $D = 2.0$, (e) $D = 3.0$.

the elastic energy decreases, and the dissipated energy increases; that is, the dissipate ratio increases and the elastic energy ratio decreases. When the stress reaches the peak value, the energy converted into elastic energy also reaches the peak value (Figures 9 and 11). Then, the tested sandstone starts to undergo overall destruction and the dissipate energy and dissipate energy ratio increase suddenly when the stress passes the peak value, while the elastic energy and elastic energy ratio show opposite change (Figures 9 and 11). In summary, the energy ratio distribution curve is in agreement with the results of stress-strain curves and energy evolution curves.

4. Conclusions

To obtain the reliable rock parameters for the underground engineering design and construction, mechanical behavior, acoustic emission properties, and energy evolution of sandstone under uniaxial compression tests considering slenderness ratio effect were quantified. The following are the main conclusions derived from the study:

(1) The greater the slenderness ratio, the smaller the peak strength and the peak strain, and the larger the elastic modulus of sandstone. A logarithmic function relationship is observed between the peak strength, the peak strain, and the elastic modulus with slenderness ratio in the tests. Besides, the sandstone would lose its load capacity without loading when the limit slenderness ratio is $D_m = 148.40$.

(2) The failure patterns of the tested sandstone varied significantly with the increasing slenderness ratio. When the slenderness ratio, D, is lower than 1.5, complex failures and multiple shear planes are formed, while simple failures and single shear planes are generated at D larger than 1.5.

(3) The AE ringing counts are more obvious with a higher slenderness ratio, D, at the initial compression stage due to the greater body volume and more defects in the sandstone.

(4) The energy evolution curves and energy ratio distribution curves can be divided into four stages, corresponding to the stress-strain curves.

Data Availability

The figures and tables data used to support the findings of this study are included within the article.

Conflicts of Interest

The authors declare that they have no conflicts of interest.

Authors' Contributions

Dai Bibo and Zhang Shuwen reviewed and edited the article and were responsible for conceptualization and methodology. Zhang Shuwen and Kang Qian wrote the original draft and performed testing and data curation. Zhao Xingdong and Zhu Zhonghua supervised the study. Dai Bibo and Zhang Shuwen reviewed and edited the article.

Acknowledgments

The authors would like to thank the Natural Science Foundation of Hunan Province (Grants nos. 2020JJ5494 and 2020JJ5490), the research project of Education Department of Hunan province (Grants nos. 18B276, 18C0439, and 19B4865), NSFC-Shandong Joint Fund (U1806208), National Key Research and Development Project (2016YFC0600803, 2018YFC0604401, and 2018YFC0604604), and the Fundamental Research Funds for the Central Universities (N2001033).

References

[1] W. J. Darlington, P. G. Ranjith, and S. K. Choi, "The effect of specimen size on strength and other properties in laboratory testing of rock and rock-like cementitious brittle materials," *Rock Mechanics and Rock Engineering*, vol. 44, no. 5, pp. 513–529, 2011.

[2] C. Zhang, P. Zou, Y. Wang, T. Jiang, H. Lin, and P. Cao, "An elasto-visco-plastic model based on stress functions for deformation and damage of water-saturated rocks during the freeze-thaw process," *Construction and Building Materials*, vol. 250, Article ID 118862, 2020.

[3] C. Y Zhang, H Lin, C. M Qiu, T. T Jiang, and J. H. Zhang, "The effect of cross-section shape on deformation, damage and failure of rock-like materials under uniaxial compression from both a macro and micro viewpoint," *International Journal of Damage Mechanics*, vol. 20, no. 7, 2020.

[4] C. Zhang, Y. Wang, and T. Jiang, "The propagation mechanism of an oblique straight crack in a rock sample and the effect of osmotic pressure under in-plane biaxial compression," *Arabian Journal of Geosciences*, vol. 13, p. 736, 2020.

[5] L. Vaisberg and E. E. Kameneva, "X-ray computed tomography in the study of physico-mechanical properties of rocks," *Gornyi Zhurnal*, vol. 9, no. 9, pp. 85–90, 2014.

[6] R. Yoshinaka, M. Osada, H. Park, T. Sasaki, and K. Sasaki, "Practical determination of mechanical design parameters of intact rock considering scale effect," *Engineering Geology*, vol. 96, no. 3-4, pp. 173–186, 2008.

[7] P. Pells, "On the absence of size effects for substance strength of Hawkesbury sandstone," *Australian Geomechanics*, vol. 39, pp. 79–83, 2004.

[8] K. Thuro, R. J. Plinninger, S. Zah, and S. Schutz, "Scale effects in rock strength properties. Part 1: unconfined compressive test and Brazilian test," *ISRM Regional Symposium Eurock 2001 Rock Mechanics a Chanllenge for Society*, vol. 3–7, pp. 169–174, 2001.

[9] R. Yoshinaka, J. Yoshida, T. Sasaki, and K. Sasaki, "Evaluation of mechanical design parameters of rock discontinuities considering scale effect," *Doboku Gakkai Ronbunshuu C*, vol. 62, no. 2, pp. 457–470, 2006.

[10] Z. P. Bazant, "Scaling theory for quasibrittle structural failure," *Proceedings of the National Academy of Sciences*, vol. 101, no. 37, pp. 13400–13407, 2004.

[11] Z. Bazant and S. Pang, "Activation energy based extreme value statistics and size effect in brittle and quasibrittle fracture," *Journal of the Mechanics & Physics of Solids*, vol. 55, no. 1, pp. 91–131, 2007.

[12] H. Masoumi, S. Saydam, and P. C. Hagan, "Incorporating scale effect into a multiaxial failure criterion for intact rock," *International Journal of Rock Mechanics and Mining Sciences*, vol. 83, pp. 49–56, 2016.

[13] C. Qi, M. Wang, J. Bai, and K. Li, "Mechanism underlying dynamic size effect on rock mass strength," *International Journal of Impact Engineering*, vol. 68, no. 7, pp. 1–7, 2014.

[14] H. R. Renani and C. D. Martin, "Modeling the progressive failure of hard rock pillars," *Tunnelling & Underground Space Technology*, vol. 74, no. 4, pp. 71–81, 2018.

[15] F. A. Steart, "Strength and stability of pillars in coal mines," *Journal of Chemical and Metallurgical Society of South Africa*, vol. 54, pp. 309–325, 1954.

[16] E. Hoek and E. T. Brown, "Practical estimates of rock mass strength," *International Journal of Rock Mechanics and Mining Sciences*, vol. 34, no. 8, pp. 1165–1186, 1997.
[17] N. M. Proskuryakov, A. A. Antonov, and V. S. Livensky, "The study of physico-mechanical properties of saliferous rocks of the starobinsky deposit," 1972.
[18] N. M. Proskuryakov, R. S. Permyakov, and A. K. Chernikov, "Physico-mechanical properties of saliferous rocks," 1973.
[19] M. Darbor, L. Faramarzi, and M. Sharifzadeh, "Size-dependent compressive strength properties of hard rocks and rock-like cementitious brittle materials," *Geosystem Engineering*, vol. 22, no. 4, pp. 179–192, 2018.
[20] I. Pankov, V. Asanov, and N. Beltyukov, "Mechanism of scale effect in saliferous rock under compression," *Procedia Engineering*, vol. 191, pp. 918–924, 2017.
[21] J. Peng, L. N. Y. Wong, and C. I. Teh, "A re-examination of slenderness ratio effect on rock strength: insights from DEM grain-based modelling," *Engineering Geology*, vol. 246, no. 28, pp. 245–254, 2018.
[22] A. B. Hawkins, "Aspects of rock strength," *Bulletin of Engineering Geology and the Environment*, vol. 57, no. 1, pp. 17–30, 1998.
[23] Z. Qi, H. H. Zhu, L. Y. Zhang, and X. B. Ding, "Study of scale effect on intact rock strength using particle flow modeling," *International Journal of Rock Mechanics & Mining Sciences*, vol. 48, pp. 1320–1328, 2011.
[24] C. Y. Liang, Q. B. Zhang, X. Li, and P. Xin, "The effect of specimen shape and strain rate on uniaxial compressive behavior of rock material," *Bulletin of Engineering Geology & the Environment*, vol. 75, no. 4, pp. 1–13, 2015.
[25] E. Tuncay and N. Hasancebi, "The effect of length to diameter ratio of test specimens on the uniaxial compressive strength of rock," *Bulletin of Engineering Geology and the Environment*, vol. 68, no. 4, pp. 491–497, 2009.
[26] S. Hai-Jian, H. W. Jing, X. B. Mao, H. H. Zhao, Q. Yin, and C. Wang, "Size effect of sandstone after high temperature under uniaxial compression," *Journal Central South University*, vol. 22, no. 5, pp. 1901–1908, 2015.
[27] K. Karaman, A. Kaya, and A. Kesimal, "Effect of the specimen length on ultrasonic P-wave velocity in some volcanic rocks and limestones," *Journal of African Earth Sciences*, vol. 112, pp. 142–149, 2015.
[28] Y. Li, D. Huang, and X. a. Li, "Strain rate dependency of coarse crystal marble under uniaxial compression: strength, deformation and strain energy," *Rock Mechanics and Rock Engineering*, vol. 47, no. 4, pp. 1153–1164, 2014.
[29] R. Ulusay, *The ISRM Suggested Methods for Rock Characterization, Testing and Monitoring: 2007-2014*, Springer, Berlin, Germany, 2015.
[30] ASTM, *Annual Book of ASTM Standards*, American Society for Testing Materials, Philadelphia, PA, USA, 2017.
[31] D. Marbor, L. Faramarzi, and M. Sharifzadeh, "Size-dependent compressive strength properties of hard rocks and rock-like cementitious brittle materials," *Geosystem Engineering*, vol. 22, no. 4, pp. 1–14, 2018.
[32] H. P. Xie, Y. Ju, and L. Y. Li, "Criteria for strength and structural failure of rocks based on energy dissipation and energy release principles," *Chinese Journal of Rock Mechanics & Engineering*, vol. 24, no. 17, pp. 3003–3010, 2005.
[33] H. P. Xie, Y. Ju, L. Y. Li, and R. D. Peng, "Energy mechanism of deformation and failure of rock masses," *Yanshilixue Yu Gongcheng Xuebao/Chinese Journal of Rock Mechanics & Engineering*, vol. 27, no. 9, pp. 1729–1740, 2008.
[34] K. Cao, L. Ma, Y. Wu, N. M. Khan, and J. Yang, "Using the characteristics of infrared radiation during the process of strain energy evolution in saturated rock as a precursor for violent failure," *Infrared Physics & Technology*, vol. 109, no. 9, Article ID 103406, 2020.
[35] F. Gao, S. Cao, K. Zhou, Y. Lin, and L. Zhu, "Damage characteristics and energy-dissipation mechanism of frozen-thawed sandstone subjected to loading," *Cold Regions Science and Technology*, vol. 169, no. 1, Article ID 102920, 2020.
[36] K. Peng, Z. Liu, Q. Zou, Q. Wu, and J. Zhou, "Mechanical property of granite from different buried depths under uniaxial compression and dynamic impact: an energy-based investigation," *Powder Technology*, vol. 362, no. 2, pp. 729–744, 2020.